Journal of Microscopy, Vol. 218, Pt 2 May 2005, pp. 171–179
Received 30 April 2004; accepted 1 February 2005

Stereological measures of trabecular bone structure: comparison of 3D micro computed tomography with 2D histological sections in human proximal tibial bone biopsies

J. S. THOMSEN*†, A. LAIB‡, B. KOLLER‡, S. PROHASKA§, LI. MOSEKILDE†¶ & W. GOWIN**

*Department of Connective Tissue Biology and †Department of Cell Biology, Institute of Anatomy, University of Aarhus, DK 8000 Århus C, Denmark

‡Scanco Medical AG, Auenring 6–8, CH-8303, Bassersdorf, Switzerland

§Zuse Institute Berlin (ZIB), Takustrasse 7, D-14195, Berlin, Germany

**Center of Muscle and Bone Research, Department of Radiology and Nuclear Medicine, Charité – University Medicine – Berlin, Joint Facility of the Freie Universität Berlin and the Humboldt-Universität zu Berlin, Benjamin Franklin Campus, Hindenburgdamm 30, D-12203, Berlin, Germany

Key words. μCT, bone structure, histology, stereology, tibia.

Summary

Stereology applied on histological sections is the 'gold standard' for obtaining quantitative information on cancellous bone structure. Recent advances in micro computed tomography (μCT) have made it possible to acquire three-dimensional (3D) data non-destructively. However, before the 3D methods can be used as a substitute for the current 'gold standard' they have to be verified against the existing standard. The aim of this study was to compare bone structural measures obtained from 3D μCT data sets with those obtained by stereology performed on conventional histological sections using human tibial bone biopsies. Furthermore, this study forms the first step in introducing the proximal tibia as a potential bone examination location by peripheral quantitative CT and CT. Twenty-nine trabecular bone biopsies were obtained from autopsy material at the medial side of the proximal tibial metaphysis. The biopsies were embedded in methylmetacrylate before μCT scanning in a Scanco μCT 40 scanner at a resolution of $20 \times 20 \times 20\ \mu m^3$, and the 3D data sets were analysed with a computer program. After μCT scanning, 16 sections were cut from the central 2 mm of each biopsy and analysed with a computerized method. Trabecular bone volume (BV/TV) and connectivity density (CD) were estimated in both modalities, whereas trabecular bone pattern factor (TBPf) was estimated on the histological sections only. Trabecular thickness (Tb.Th), number (Tb.N) and separation (Tb.Sp), and structure model index (SMI) were estimated with the μCT method only. Excellent correlations were found between the two techniques for BV/TV ($r = 0.95$) and CD ($r = 0.95$). Additionally, an excellent relationship ($r = 0.95$) was ascertained between TBPf and SMI. The study revealed high correlations between measures of bone structure obtained from conventional 2D sections and 3D μCT data. This indicates that 3D μCT data sets can be used as a substitute for conventional histological sections for bone structural evaluations.

Introduction

It has been suggested that the loss of trabecular bone strength and the resulting increased risk of bone fractures depends not only on the loss of trabecular bone density, but also on the loss of structural elements as well as a loss of connectivity (Kleerekoper *et al.*, 1985; Goldstein, 1987; Parfitt, 1987; Mosekilde, 1988, 1989, 1993; Ciarelli *et al.*, 1991; Delling & Amling, 1995; Majumdar *et al.*, 1998; Gomberg *et al.*, 2000). Consequently, it is important when investigating pathological, age-related, treatment-induced or immobilization-induced changes in trabecular bone to ascertain not only the changes in bone density but also the changes in bone structure.

The 'gold standard' for investigating trabecular bone structure is the application of stereological methods to histological sections (Weibel, 1980). Recent advances in micro computed tomography (μCT) and magnetic resonance imaging (MRI) have made it feasible to perform three-dimensional (3D) evaluations non-destructively (Feldkamp *et al.*, 1989; Kuhn *et al.*, 1990; Bonse *et al.*, 1994; Chung *et al.*, 1995; Rüegsegger *et al.*, 1996; Engelke *et al.*, 1999; Gomberg *et al.*, 2000; Wehrli *et al.*, 2002).

Correspondence to: Dr Jesper Thomsen. Tel.: +45 8942 3015; fax: +45 8613 7539; e-mail: jesper@jst.ana.au.dk.

¶Her coauthors would like to pay tribute to Lis, who sadly died before the study was completed.

However, before these non-destructive 3D methods can be used as a substitute for the current 'gold standard' it is important to compare in a controlled setting the results obtained by the 3D methods with those obtained by established mathematically sound stereological methods based on 2D sections.

The present study forms part of a larger investigation into the influence of microgravity on trabecular bone structure in general. One of the goals of our investigations is to be able to quantify structural changes of the skeleton when exposed to microgravity. Another important goal of the research project is to find a suitable skeletal location appropriate for ascertaining the bone status of space-flying personnel. As the largest changes of bone mass after exposure to microgravity have been found at the load-bearing lower extremities (Vico *et al.*, 2000) and in the axial skeleton (LeBlanc *et al.*, 2000), a bone status examination should ideally include these sites. The proximal tibial metaphysis was chosen as it is the most easily accessible site for non-invasive quantification of the bone structure by peripheral quantitative CT (pQCT) or whole-body CT, and as it is also as rich in trabecular bone tissue as a lumbar vertebral body. However, because this skeletal site is new for radiological bone assessment we started at the microscopic level of trabecular structure evaluation in order to establish the suitability of this site for non-invasive bone status assessments. A recently published research project evaluating trabecular microarchitecture in men with spinal cord injury also used the proximal tibial metaphysis as a site for MRI-based structural assessments (Modlesky *et al.*, 2004).

This approach required obtaining bone biopsies at an unconventional location. However, the proximal tibial metaphysis with its rich trabecular network is used as a donor site for bone grafting (O'Keeffe *et al.*, 1991; Catone *et al.*, 1992; Alt *et al.*, 1999; Hughes & Revington, 2002), which illustrates that it is feasible to obtain cancellous bone at this site. Moreover, Sivarajasingam *et al.* (2001) compared the iliac crest and the proximal tibia as donor grafting sites and showed that bone healing at the tibial site is faster than at the iliac crest. However, we want to avoid giving the impression that the proximal tibia should be used as a site for the collection of bone biopsies, although this would be feasible and would lead to excellent results, but it should be borne in mind that this is a surgical procedure requiring many more precautions than taking bone biopsies at the common iliac crest site.

The aim of the present study was therefore to compare measures of bone structure estimated from 3D μCT data sets with the 'gold standard' of stereology applied to histological sections obtained from human tibial biopsies in order to ascertain how well the 3D data sets acquired by μCT quantify the bone structure.

Materials and methods

Bone specimens

Our space research project had access to 30 individuals. At autopsy, the specimens were placed in formalin for fixation. One sample was excluded as subsequent analyses found signs of vertebral bone manifestation of leukaemia. The remaining 29 individuals comprised the population used in the current study (19 women aged 57–98 years and ten men aged 60–94 years).

The medial side of the proximal tibial metaphysis was chosen rather than the lateral side as it has been shown that the medial side bears up to 75% of the load of the knee (Hsu *et al.*, 1990), and it is therefore reasonable to assume that the medial side is more sensitive to skeletal unloading. Furthermore, the trabecular structure at the lateral side of the proximal tibial metaphysis is less well defined than at the medial side, owing to the particular biomechanics of the tibiofibular articulation.

Specimen preparation

Cylindrical bone samples with a diameter of 7 mm were obtained 14 mm distal from the centre of the medial facet of the superior articular surface by drilling with a compressed-air-driven drill with a diamond-tipped trephine at either the right or the left proximal tibial metaphysis. The drilling and the localization of the correct position were performed under fluoroscopy. The length axis of the biopsy was exactly perpendicular to the length axis of the tibia and exactly parallel to the frontal vertical plane. This biopsy position within the proximal tibial metaphysis was selected in order to avoid interference with remains of the epiphyseal growth plate ('epiphyseal scar'). The length of the biopsies varied between approximately 2 cm and 5 cm.

The biopsies were first rinsed in water and then placed in increasing concentrations of ethanol solutions in order to wash out the formalin. The samples were degassed in an exicator immediately before they were embedded in methylmethacrylate. The biopsies were embedded in test tubes with an inner diameter of 14.5 mm in order to limit the amount of excess embedding material. This made it possible to perform μCT on the samples at a high resolution while retaining the ability to cut sections from the embedded samples.

Micro computed tomography and stereology

The embedded bone biopsies were scanned without further sample preparation in a desktop MicroCT (μCT-40, Scanco Medical, Bassersdorf, Switzerland; http://www.microct.com) with a resolution of $20 \times 20 \times 20\ \mu m^3$ (X-ray voltage 70 kV_p). The resolution of 20 μm was chosen in favour of a resolution of 10 μm owing to the latter resulting in unmanageably huge amounts of data combined with the fact that Müller *et al.* (1996) have shown that resolutions up to 60 μm in μCT scanners can produce morphometric results for human bone biopsies similar to those obtained with a resolution of 10 μm. A resolution of 20 μm was thus considered adequate without invalidating a comparison with stereology performed on 2D sections obtained at a section thickness and pixel size of 10 μm. The entire length of the bone cylinder was scanned with up to

2000 transverse slices per biopsy, where each slice consisted of 1024×1024 pixels. This virtual-slicing direction perpendicular to the main axis of the biopsy was necessary to achieve the high resolution. Because all slices were obtained consecutively and a complete 3D reconstruction was performed before any quantifying assessment, the slicing direction did not have an influence on the integrity of the 3D data set itself. For the numerical analyses, a volume of interest (VOI) approximately 0.5 mm smaller than the radius of the cylindrical biopsies was chosen in order to exclude accumulated drilling residue around the outer layer. The resulting entire 3D data set was segmented using a low-pass filter to remove noise, and a fixed threshold filter to extract the mineralized bone phase. The threshold was set to 17.5% of the maximum 2-byte value, which is equivalent to a 5734 greyscale value out of a maximum of 32 767. This threshold corresponds to a linear attenuation coefficient of 1.4 cm^{-1} at 70 kV_p. This is comparable to 64% of the bone level, which had an average linear attenuation coefficient of 2.2 cm^{-1}. From the binarized 3D data set, the trabecular bone network was quantified with two different second-order stereology (Howard & Reed, 1998) techniques.

First, a 'direct' 3D technique without model assumptions of the appearance of trabecular bone was applied. Trabecular bone volume (BV/TV) was computed using voxel counting. Trabecular number (Tb.N*), thickness (Tb.Th*) and separation (Tb.Sp*) were obtained by measuring 3D distances directly in the trabecular network using the method of Hildebrand & Rüegsegger (1997a). The asterisks indicate that the measures have been computed using the direct method. Tb.Th* was determined as the diameter of spheres filling the bone structures, Tb.Sp* was determined as the diameter of spheres filling the marrow spaces and Tb.N* was determined as the inverse of the mean distances of the skeletonized bone structure (Hildebrand *et al.*, 1999). Furthermore, connectivity density (CD) was determined using a method based on Euler numbers described by Odgaard (1997) and Odgaard & Gundersen (1993).

Next, the bone surface was triangulated using a tetrahedron meshing technique involving the marching cube algorithm (Lorensen & Cline, 1987). Using the parallel-plate model assumption (Parfitt *et al.*, 1983), Tb.Th, Tb.Sp and Tb.N were determined from bone surface area (BS), bone volume (BV), marrow volume (MV) and total tissue volume (TV) as described by Hildebrand *et al.* (1999) and Laib & Rüegsegger (1999):

$$\mathrm{Tb.Th} = 2\frac{\mathrm{BV}}{\mathrm{BS}} \tag{1}$$

$$\mathrm{Tb.N} = \frac{1}{2}\frac{\mathrm{BS}}{\mathrm{TV}} \tag{2}$$

$$\mathrm{Tb.Sp} = 2\frac{\mathrm{MV}}{\mathrm{BS}} \tag{3}$$

The structure model index (SMI) was determined using the method by Hildebrand & Rüegsegger (1997b):

$$\mathrm{SMI} = 6\frac{\mathrm{BV}}{\mathrm{BS}^2}\frac{d\mathrm{BS}}{dr} \tag{4}$$

where $d\mathrm{BS}/dr$ denotes the bone surface area derived with respect to a linear measure r in such a way that $\mathrm{BS} = \partial\mathrm{BV}/\partial r$. The surface area derivative $d\mathrm{BS}/dr$ was estimated by first finding the bone surface area $\mathrm{BS}(r)$, then simulating a thickening of the trabecular bone structure by translating the triangulated surface by a small distance Δr in its normal direction, and finally determining the bone surface area $\mathrm{BS}(r + \Delta r)$. The surface area derivative is then estimated by:

$$\frac{d\mathrm{BS}}{dr} = \frac{\mathrm{BS}(r + \Delta r) - \mathrm{BS}(r)}{\Delta r} \tag{5}$$

where the thickening of the trabecular structure Δr was selected so that it was more than an order of magnitude smaller than the voxel side length (Hildebrand & Rüegsegger, 1997b).

The SMI quantifies the plate vs. rod characteristics of trabecular bone, where a purely plate-like trabecular structure has an SMI of 0, a purely rod-like trabecular structure has an SMI of 3, and a trabecular structure consisting of both plate-like and rod-like trabeculae has an SMI value between 0 and 3.

Three-dimensional reconstruction and visualization was performed using the visualization system Amira 3.1 (Stalling *et al.*, 2005).

Two-dimensional sectioning and stereology

The trabecular bone of the proximal tibial metaphysis is anisotropic (Ding *et al.*, 2002) where the main trabecular orientation is cranial–caudal in the frontal vertical plane. This main orientation of the trabeculae in the biopsies was found using μCT scans, and the direction was marked on the embedded bone samples with a permanent marker pen, enabling sectioning of the biopsies in a known anatomical direction. The cutting direction was parallel to the main axis of the biopsy and perpendicular to the main orientation of the trabeculae. Although the use of a fixed section direction introduced a bias, it was suggested that in this way the results would be representative for the main loading direction of the tibia.

The samples were cut in 10-μm-thick frontal sections on a Jung model K microtome (R. Jung GmbH, Heidelberg, Germany) from the central 2 mm of each biopsy. Two 10-μm-thick sections separated by 10 μm formed a disector pair (Sterio, 1984; Gundersen *et al.*, 1993). Six consecutive sections were cut, stained and mounted. From these four possible disector pairs, the pair with the fewest sectioning artefacts was selected for further analysis. The distance between two sets of six consecutive sections was 180 μm. In all, 16 sections were analysed per biopsy, thus covering the central 2 mm of each biopsy. All sections were stained with aniline blue (modified Masson trichrome).

The mounted 10-μm-thick aniline-blue-stained sections were placed in an Agfa Arcus II image scanner (Agfa-Gevaert AG,

Leverkusen, Germany) with an integrated transparency scanning unit. Digital images of the sections were acquired with Agfa Fotolook 2.09 (Agfa-Gevaert AG) in the 'line art' setting (1-bit images) at a resolution of 2540 dpi (pixel size $10 \times 10\ \mu m^2$). The threshold used during image scanning was determined by scanning one bone section at different thresholds and selecting by visual inspection in a stereo microscope (Olympus SZ-40, Olympus, Tokyo, Japan) the threshold that resulted in the closest resemblance of the digitized image to the bone section.

The GNU Image Manipulation Program (GIMP) (http://www.gimp.org), running under the Linux operating system (Red Hat Linux 6.2, Red Hat Software, Inc., Raleigh, NC, U.S.A.) was used to remove artefacts from the images. During removal of artefacts, comparison was made between the computerized image and the section using the stereo microscope.

Thomsen *et al.* (2000) have previously described the computer program used for the stereological analysis of the sections in detail. Nevertheless, the relevant functions are briefly described in the following. The computer program presented the digitized image on the computer screen so that a polygon-shaped region of interest (ROI) could be drawn in the same way as the VOI for the μCT data.

The bone volume fraction [trabecular bone volume, BV/TV (B.Ar/T.Ar)] was determined as the number of pixels representing the bone area divided by the number of pixels representing the combined bone and marrow area. The bone area (B.Ar), marrow area (M.Ar) and tissue area (T.Ar) could thereafter be determined, as the area of one pixel is $10 \times 10\ \mu m^2 = 100\ \mu m^2$.

The trabecular bone pattern factor (TBPf) was determined using the method described by Hahn *et al.* (1992): the bone area (B.Ar) and the length of the bone perimeter (B.Pm) are determined. The bone is dilated by applying a median filter to the binary image, thereby thickening the trabecular structure with one pixel. The bone area (B.Ar′) and the length of the bone perimeter (B.Pm′) are then determined again. The trabecular bone pattern factor is defined as:

$$\mathrm{TBPf} = \frac{\Delta \mathrm{B.Pm}}{\Delta \mathrm{B.Ar}} = \frac{\mathrm{B.Pm'} - \mathrm{B.Pm}}{\mathrm{B.Ar'} - \mathrm{B.Ar}} \qquad (6)$$

The digitized images with the ROI superimposed were exported from the computer program and printed on paper. The connectivity density was determined by use of the ConnEulor principle (Gundersen *et al.*, 1993; Youngs *et al.*, 1994) comparing the printed images of the sections forming a disector pair.

Statistics

Linear regression was performed using custom-made software, whereas comparison of the mean values of the sectioning-derived measures with the 3D μCT measures was performed with a paired samples *t*-test using SPSS version 10.0 (SPSS, Chicago, IL, U.S.A.).

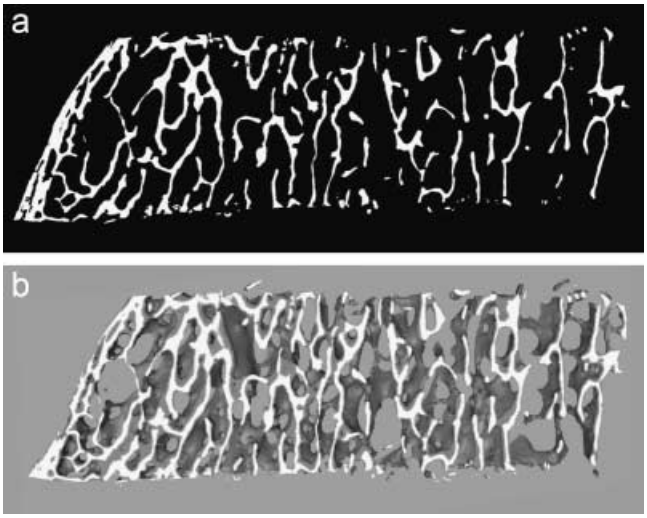

Fig. 1. (a) A single section originating from one of the proximal tibial biopsies. The colours of the section have been inverted in order to facilitate an easy comparison with the 3D reconstruction shown in (b). (b) A 3D reconstruction of the proximal tibial biopsy. Only the part of the biopsy that lies beneath the section shown in (a) has been reconstructed. The surface of the reconstructed region is very similar to the section in (a).

Results

Figure 1(a) shows a section from one of the proximal tibial biopsies, whereas Fig. 1(b) shows the same region but reconstructed from the 3D μCT data. The bone tissue that lies beneath the surface cut shown in white has been 3D reconstructed so that the region can be seen in its structural context. The surface of the 3D reconstruction appears very similar to the 2D section.

BV/TV estimated from 3D μCT has been plotted in Fig. 2(a) as a function of BV/TV assessed from sections. The regression coefficients and the correlation coefficient for the relationship are given in Table 1. The relationship between BV/TV determined from 3D μCT data and 2D sections was excellent ($r = 0.95$). Furthermore, the slope of the fit-line was not significantly different from 1, and the *y*-axis intercept was not

Table 1. Regression coefficients (α and β), correlation coefficients (*r*) and levels of significance (*P*) for the relationships ($y = \alpha x + \beta$) between the stereological measures obtained from either 2D sections or 3D μCT data sets.

Measure						
2D (*x*)	3D (*y*)	α	β	*r*	*P*	Fig.
BV/TV	BV/TV	0.946	−0.006%	0.95	1.02×10^{-15}	2a
CD	CD	0.819[a]	0.660 mm^{-3} [b]	0.95	2.28×10^{-15}	2b
TBPf	SMI	0.307 mm[a]	0.471[b]	0.95	8.38×10^{-15}	2c

[a]Slope (α) significantly ($P < 0.05$) different from 1; [b]*y*-axis intercept (β) significantly ($P < 0.05$) different from 0. $n = 29$.

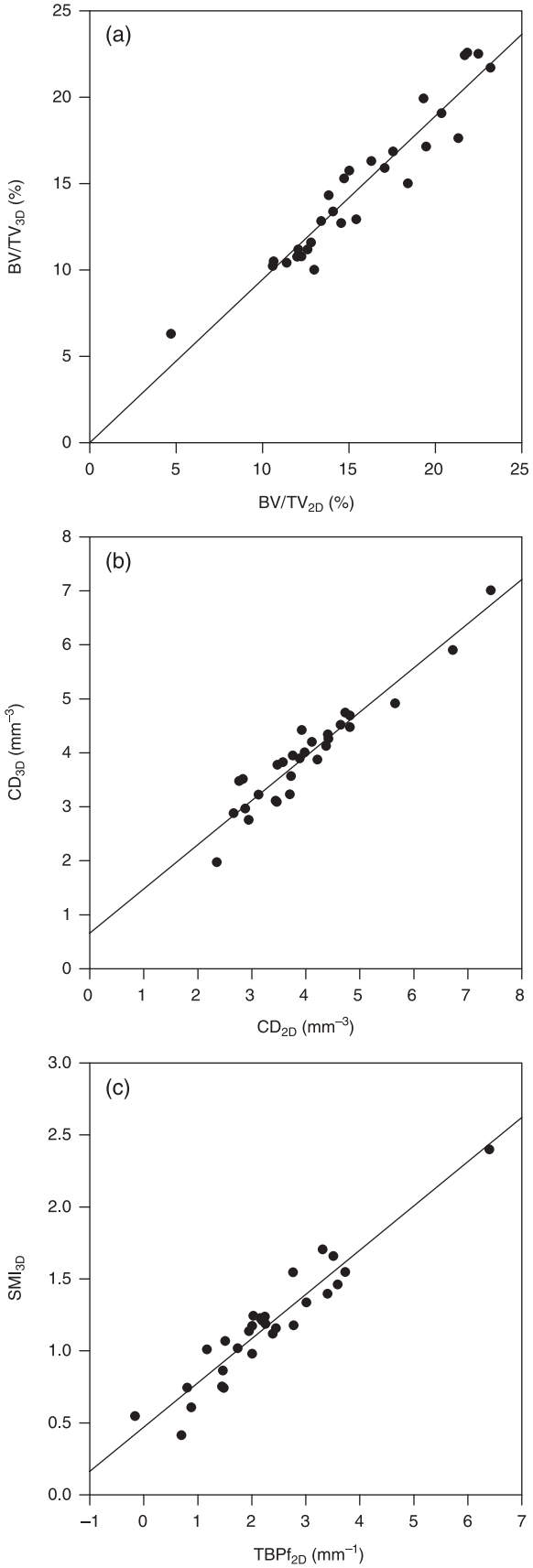

Table 2. Regression coefficients (α and β), correlation coefficients (r) and levels of significance (P) for the relationships ($y = \alpha x + \beta$) between directly estimated 3D measures and model-based 3D measures.

3D measure						
Direct (x)	Model (y)	α	β	r	P	Fig.
Tb.Th*	Tb.Th	0.762[a]	4.51 µm	0.95	1.82×10^{-15}	3a
Tb.N*	Tb.N	1.401[a]	−0.492 mm^{-1} [b]	0.87	5.51×10^{-10}	3b
Tb.Sp*	Tb.Sp	1.425[a]	−375.5 µm[b]	0.84	1.46×10^{-8}	3c

[a]Slope (α) significantly ($P < 0.05$) different from 1; [b]y-axis intercept (β) significantly ($P < 0.05$) different from 0. $n = 29$.

significantly different from 0, indicating that the levels of BV/TV detected by the two methods are similar.

Figure 2(b) shows the connectivity density determined directly from 3D µCT data plotted as a function of connectivity density determined by design-based stereology from disector pairs. An excellent correlation ($r = 0.95$) was also found between the two techniques for CD. However, the slope of the regression line was significantly different from 1 ($P = 0.0014$), and the y-axis intercept was significantly different from 0 ($P = 0.0044$).

In Fig. 2(c) the structure model index estimated from 3D µCT data is shown as a function of trabecular bone pattern factor determined from 2D sections. An excellent correlation was found between SMI and TBPf ($r = 0.95$), which is remarkable given that SMI is not the exact 3D representation of TBPf.

Figure 3 shows trabecular thickness, trabecular number and trabecular separation ascertained by the 3D version of the parallel-plate model plotted against the corresponding directly estimated measures. The regression and correlation coefficients for these relationships are given in Table 2. For all relationships it was found that the slope of the regression line was significantly different from 1. Additionally, the y-axis intercept for the regression line was significantly different from 0 for trabecular number and separation, indicating an offset between the estimates of trabecular number and separation determined by the two methods.

Table 3 shows the mean value of BV/TV and CD obtained by either stereology performed on 2D sections or 3D µCT data sets. There exists a significant offset between the mean values ascertained by the two techniques for BV/TV, whereas the offset did not reach the level of significance for CD.

Table 4 compares the average values of the parameters estimated by either the 3D parallel-plate model-based method

Fig. 2. (a) Trabecular bone volume estimated from µCT data sets (BV/TV_{3D}) plotted against trabecular bone volume estimated from 2D sections (BV/TV_{2D}). (b) Connectivity density estimated from µCT data sets (CD_{3D}) plotted against connectivity density estimated with the ConnEulor principle (CD_{2D}). (c) Structure model index estimated from µCT data sets (SMI_{3D}) plotted against trabecular bone pattern factor estimated from 2D sections ($TBPf_{2D}$). All relationships are highly significant with correlation coefficients of $r = 0.95$ (Table 1).

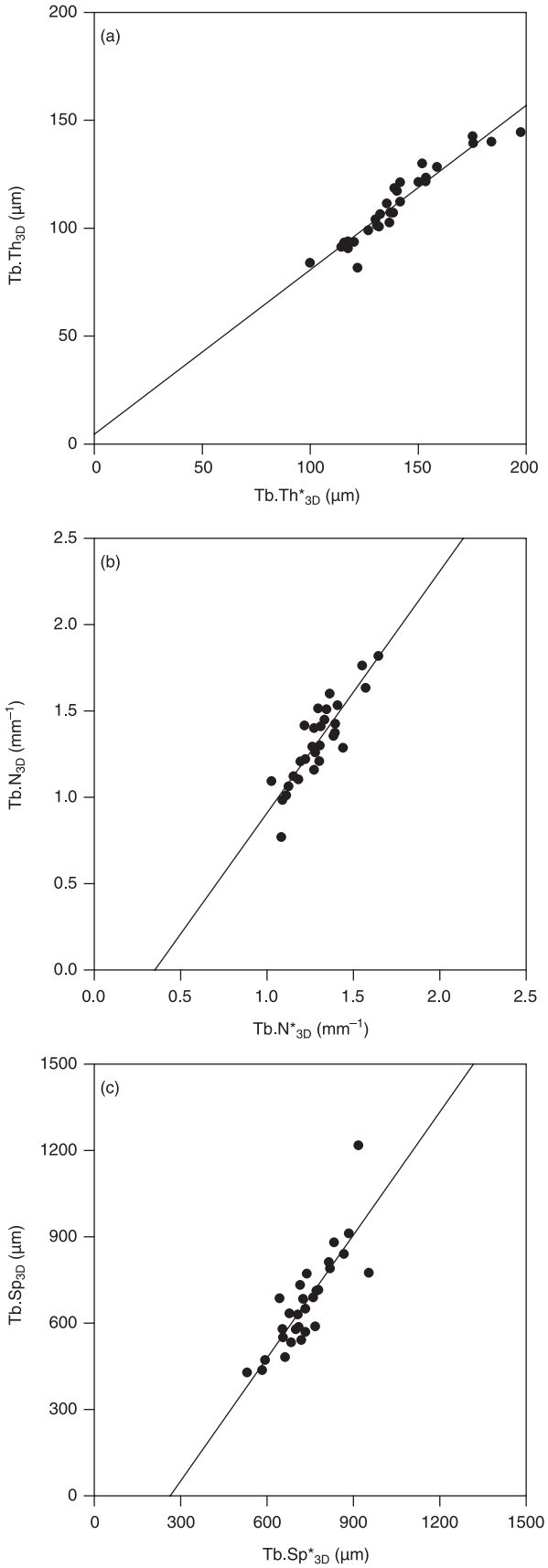

or the direct 3D method. It was found that the mean value of trabecular thickness and trabecular separation obtained by either the direct 3D method or the 3D version of the parallel-plate model differed significantly, whereas the difference in the mean values did not reach the level of significance for trabecular number.

Discussion

This study has shown that there is a very good correlation between the bone structural measures obtained from 3D μCT data sets and from stereology performed on 2D sections. Excellent correlations were found for BV/TV and CD. An excellent correlation was also revealed between the 3D measure SMI and the 2D measure TBPf. This study is the first to compare 3D μCT assessments with conventional 2D section-based measures on trabecular bone samples obtained from the proximal tibial metaphysis.

Uchiyama *et al.* (1997) determined the relationship between BV/TV estimated by μCT and stereology at the iliac crest and obtained a strong correlation between the two measures ($r = 0.95$). Likewise, Müller *et al.* (1998) found a strong correlation ($r = 0.93$) between BV/TV values determined from μCT data sets and stereology on histological sections at the iliac crest. In contrast, a somewhat weaker correlation ($r = 0.71$) between the two measurement techniques was ascertained by Ito *et al.* (1998) at the iliac crest. Cendre *et al.* (1999) compared BV/TV values obtained by section-based stereology and high-resolution CT on vertebral bone biopsies and found a Spearman rank correlation of $\rho = 0.84$, whereas Banse *et al.* (2002) compared pQCT with stereology conducted on vertebral bone samples and established a correlation coefficient of $r = 0.93$ for BV/TV. The correlation between BV/TV values obtained from μCT data sets and from sections found in the present study is thus either equal to or greater than the previously reported findings. These results reveal that high-resolution μCT is able to produce BV/TV values of quality equal to those obtained with the current 'gold standard' of stereology performed on histological sections. However, it was also demonstrated that on average the 2D section-based method estimated slightly higher values of BV/TV than those obtained from 3D μCT data sets.

The present study has elucidated an excellent correlation between connectivity density estimated by use of the ConnEulor principle (Gundersen *et al.*, 1993; Youngs *et al.*, 1994) and a direct 3D estimation. The present study is, to the best of our knowledge, the first to conduct a comparison of connectivity density determined by the ConnEulor method with a direct 3D method. The correlation we have found between CD estimated

Fig. 3. Three-dimensional parallel-plate model-based estimated measures plotted against direct 3D estimated measures. (a) Trabecular thickness (Tb.Th), (b) trabecular number (Tb.N) and (c) trabecular separation (Tb.Sp). An asterisk denotes that the measure is determined directly. Regression and correlation coefficients for the relationships are given in Table 2.

Table 3. Mean values of BV/TV and CD obtained from either 2D sections or 3D μCT data sets. The difference between the mean values and the levels of significance (*P*) of the comparison (paired samples *t*-test) of the mean values of the applied measurement techniques are also listed.

2D		3D			
Measure	Mean	Measure	Mean	Difference	*P*
BV/TV	15.585%	BV/TV	14.738%	−5.43%	1.74×10^{-3}
CD	4.0289 mm^{-3}	CD	3.9584 mm^{-3}	−1.75%	N.S.

Table 4. Mean values of the various stereological measures estimated by either the direct 3D method or the model-based 3D method. The difference between the mean values and the levels of significance (*P*) of the comparison (paired samples *t*-test) of the mean values of the two measurement techniques are also listed.

Direct 3D		Parallel-plate 3D			
Measure	Mean	Measure	Mean	Difference	*P*
Tb.Th*	140.28 μm	Tb.Th	111.44 μm	−20.56%	2.22×10^{-16}
Tb.N*	1.2937 mm^{-1}	Tb.N	1.3205 mm^{-1}	2.07%	N.S.
Tb.Sp*	735.23 μm	Tb.Sp	671.95 μm	−8.61%	2.02×10^{-3}

by the 3D method and the ConnEulor method illustrates that it is possible to obtain 3D structural information from 2D sections provided that the 2D analysis is carried out in an appropriate manner.

Recent studies have indicated that the 3D version of the parallel-plate model underestimates the trabecular thickness estimated by direct 3D methods by up to 30–40% (Hildebrand *et al.*, 1999; Kothari *et al.*, 1999; Day *et al.*, 2000; Ding & Hvid, 2000). These findings are confirmed by the present study, where we found an underestimation of the trabecular thickness of 21% by the model-based method compared with the direct method.

The present study has revealed an excellent correlation between TBPf derived from histological sections and SMI acquired from 3D μCT data sets. This finding is supported by the study of Ikeda *et al.* (2001), which obtained a correlation coefficient between TBPf and SMI of $r = 0.98$ in rat vertebrae. This tight relationship between TBPf and SMI indicates that the physical interpretation of TBPf may be similar to that of SMI, i.e. a quantification of the balance between rod-like and plate-like trabecular structures. However, this relationship between SMI and TBPf is also somewhat puzzling, as SMI is dimensionless, whereas TBPf has a unit of mm^{-1}. This might indicate that the relationship is of an empirical rather than a theoretical nature.

Shrinkage during the cutting process will inevitably lead to inherent differences between the μCT-based and the section-based measures. Uchiyama *et al.* (1997) showed shrinkage of 17.66% perpendicular to the knife and 2.29% parallel to the knife in iliac crest bone biopsies. When performing estimations using histological sections, shrinkage is not normally taken into consideration, and we therefore believe that it would not be appropriate to correct for shrinkage in this comparative study either, as to do so may lead to an overestimation of the strength of the relationships.

Even though our study has shown that it is feasible to conduct structural evaluations with 3D μCT, it should be borne in mind that this technique is currently limited to static assessments only. In contrast, appropriately prepared bone sections can be used for either static or dynamic assessments.

Patel *et al.* (2003) have recently shown how the trabecular bone structure changes with the distance from the knee joint in the proximal tibial metaphysis. They found that the trabecular bone structure changed rapidly in the first 6–8 mm under the knee joint, after which it stabilized and was then almost independent of the distance to the knee joint. The biopsies used in the present study were obtained 14 mm distal from the knee joint, which coincides with the region of stable trabecular structure determined by Patel *et al.* (2003), thus illustrating the suitability of our biopsy location for structural analysis.

In conclusion, the present study has revealed an excellent correlation between key bone measures of bone structure estimated by stereology applied to histological sections and by 3D μCT. This indicates – in conjunction with the results shown in previously published studies (Uchiyama *et al.*, 1997; Ito *et al.*, 1998; Müller *et al.*, 1998; Cendre *et al.*, 1999; Banse *et al.*, 2002) – that if proper care is taken, 3D μCT can be used as a substitute for section-based stereological methods for describing the trabecular bone architecture. However, the 3D μCT technique cannot, at present, be used for dynamical bone assessments. Furthermore, the study has empirically verified the stereological ConnEulor method for determining connectivity density. This study also indicates that the proximal tibial metaphysis could potentially be used for assessing the structure of weight-bearing trabecular bone.

Acknowledgements

We are grateful for the excellent technical assistance of Inger Vang Magnussen, Institute of Anatomy, University of Aarhus, Århus, Denmark. Michael Hewitt is gratefully acknowledged for linguistic revision of this manuscript. Professor G. Bogusch, Institute of Anatomy, Campus Mitte, and Professor R. Graf, Institute of Anatomy, Campus Benjamin Franklin of the Joint Facility of the Freie Universität Berlin and the Humboldt-Universität zu Berlin, Charité – University Medicine – Berlin,

are acknowledged for kindly providing the bone specimens. The help of Dr Michael Giehl was instrumental for finding the correct cutting direction by using the cone beam-based μCT equipment available at the Center of Muscle and Bone Research, Charité – University Medicine – Berlin, Joint Facility of the Freie Universität Berlin and the Humboldt-Universität zu Berlin, Campus Benjamin Franklin, Berlin, Germany. Professor A. Michael Parfitt and Dr Michael Amling are acknowledged for help in ascertaining the sectioning direction in the proximal tibial metaphysis. This study was made possible in part by grants from the Microgravity Application Program (Biotechnology) from the Manned Spaceflight Program of the European Space Agency (ESA). We would also like to acknowledge Scanco Medical AG, Roche Pharmaceuticals and Siemens AG for support of the study.

References

Alt, V., Nawab, A. & Seligson, D. (1999) Bone grafting from the proximal tibia. *J. Trauma*, **47**, 555–557.

Banse, X., Devogelaer, J.P. & Grynpas, M. (2002) Patient-specific microarchitecture of vertebral cancellous bone: a peripheral quantitative computed tomographic and histological study. *Bone*, **30**, 829–835.

Bonse, U., Busch, F., Günnewig, O., Beckmann, F., Pahl, R., Delling, G., Hahn, M. & Graeff, W. (1994) 3D computed X-ray tomography of human cancellous bone at 8 μm spatial and 10^{-4} energy resolution. *Bone Miner*. **25**, 25–38.

Catone, G.A., Reimer, B.L., McNeir, D. & Ray, R. (1992) Tibial autogenous cancellous bone as an alternative donor site in maxillofacial surgery: a preliminary report. *J. Oral Maxiliofac. Surg*. **50**, 1258–1263.

Cendre, E., Mitton, D., Roux, J.-P., Arlot, M.E., Duboeuf, F., Burt-Pichat, B., Rumelhart, C., Peix, G. & Meunier, P.J. (1999) High-resolution computed tomography for architectural characterization of human lumbar cancellous bone: relationships with histomorphometry and biomechanics. *Osteoporos. Int*. **10**, 353–360.

Chung, H.-W., Wehrli, F.W., Williams, J.L., Kugelmass, S.D. & Wehrli, S.L. (1995) Quantitative analysis of trabecular microstructure by 400 MHz nuclear magnetic resonance imaging. *J. Bone Miner. Res*. **10**, 803–811.

Ciarelli, M.J., Goldstein, S.A., Kuhn, J.L., Cody, D.D. & Brown, M.B. (1991) Evaluation of orthogonal mechanical properties and density of human trabecular bone from the major metaphyseal regions with materials testing and computed tomography. *J. Orthop. Res*. **9**, 674–682.

Day, J.S., Ding, M., Odgaard, A., Sumner, D.R., Hvid, I. & Weinans, H. (2000) Parallel plate model for trabecular bone exhibits volume fraction-dependent bias. *Bone*, **27**, 715–720.

Delling, G. & Amling, M. (1995) Biomechanical stability of the skeleton – it is not only bone mass, but also bone structure that counts. *Nephrol. Dial. Transplant*. **10**, 601–606.

Ding, M. & Hvid, I. (2000) Quantification of age-related changes in the structure model type and trabecular thickness of human tibial cancellous bone. *Bone*, **26**, 291–295.

Ding, M., Odgaard, A., Linde, F. & Hvid, I. (2002) Age-related variations in the microstructure of human tibial cancellous bone. *J. Orthop. Res*. **20**, 615–621.

Engelke, K., Karolczak, M., Lutz, A., Seibert, U., Schaller, S. & Kalender, W. (1999) Mikro-CT. Technologie und Applikationen zur Erfassung von Knochenarchitektur. *Radiologe*, **39**, 203–212.

Feldkamp, L.A., Goldstein, S.A., Parfitt, A.M., Jesion, G. & Kleerekoper, M. (1989) The direct examination of three-dimensional bone architecture in vitro by computed tomography. *J. Bone Miner. Res*. **4**, 3–11.

Goldstein, S.A. (1987) The mechanical properties of trabecular bone: dependence on anatomic location and function. *J. Biomech*. **11/12**, 1055–1061.

Gomberg, B.R., Saha, P.K., Song, H.K., Hwang, S.N. & Wehrli, F.W. (2000) Topological analysis of trabecular bone MR images. *IEEE Trans. Med. Imaging*, **19**, 166–174.

Gundersen, H.J.G., Boyce, R.W., Nyengaard, J.R. & Odgaard, A. (1993) The ConnEulor: unbiased estimation of connectivity using physical disectors under projection. *Bone*, **14**, 217–222.

Hahn, M., Vogel, M., Pompesius-Kempa, M. & Delling, G. (1992) Trabecular bone pattern factor – a new parameter for simple quantification of bone microarchitecture. *Bone*, **13**, 327–330.

Hildebrand, T., Laib, A., Müller, R., Dequeker, J. & Rüegsegger, P. (1999) Direct three-dimensional morphometric analysis of human cancellous bone: microstructural data from spine, femur, iliac crest, and calcaneus. *J. Bone Miner. Res*. **14**, 1167–1174.

Hildebrand, T. & Rüegsegger, P. (1997a) A new method for the model-independent assessment of thickness in three-dimensional images. *J. Microsc*. **185**, 67–75.

Hildebrand, T. & Rüegsegger, P. (1997b) Quantification of bone microarchitecture with the structure model index. *Comput. Meth. Biomech. Biomed. Engin*. **1**, 15–23.

Howard, C.V. & Reed, M.G. (1998) *Unbiased Stereology*. Bios Scientific, Oxford.

Hsu, R.W., Himeno, S., Coventry, M.B. & Chao, E.Y.S. (1990) Normal axial alignment of the lower extremity and load-bearing distribution at the knee. *Clin. Orthop*. **255**, 215–227.

Hughes, C.W. & Revington, P.J. (2002) The proximal tibia donor site in cleft alveolar bone grafting: experience of 75 consecutive cases. *J. Cranio-Maxillofac. Surg*. **30**, 12–16.

Ikeda, S., Tsurukami, H., Ito, M., Sakai, A., Sakata, T., Nishida, S., Takeda, S., Shiraishi, A. & Nakamura, T. (2001) Effect of trabecular bone contour on ultimate strength of lumbar vertebra after bilateral ovariectomy in rats. *Bone*, **28**, 625–633.

Ito, M., Nakamura, T., Matsumoto, T., Tsurusaki, K. & Hayashi, K. (1998) Analysis of trabecular microarchitecture of human iliac bone using microcomputed tomography in patients with hip arthrosis with or without vertebral fracture. *Bone*, **23**, 163–169.

Kleerekoper, M., Villanueva, A.R., Stanciu, J., Sudhaker Rao, D. & Parfitt, A.M. (1985) The role of three-dimensional trabecular microstructure in the pathogenesis of vertebral compression fractures. *Calcif. Tissue Int*. **37**, 594–597.

Kothari, M., Keaveny, T.M., Lin, J.C., Newitt, D.C. & Majumdar, S. (1999) Measurement of intraspecimen variations in vertebral cancellous bone architecture. *Bone*, **25**, 245–250.

Kuhn, J.L., Goldstein, S.A., Feldkamp, L.A., Goulet, R.W. & Jesion, G. (1990) Evaluation of a microcomputed tomography system to study trabecular bone structure. *J. Orthop. Res*. **8**, 833–842.

Laib, A. & Rüegsegger, P. (1999) Calibration of trabecular bone structure measurements of in vivo three-dimensional peripheral quantitative computed tomography with 28-μm-resolution microcomputed tomography. *Bone*, **24**, 35–39.

LeBlanc, A., Schneider, V., Shackelford, L., West, S., Oganov, V., Bakulin, A. & Voronin, L. (2000) Bone mineral and lean tissue loss after long duration space flight. *J. Musculoskel. Neuron. Interact*. **1**, 157–160.

Lorensen, W.E. & Cline, H.E. (1987) Marching cubes: a high resolution 3D surface construction algorithm. *Comput. Graph*. **21**, 163–169.

Majumdar, S., Kothari, M., Augat, P., Newitt, D.C., Link, T.M., Lin, J.C., Lang, T., Lu, Y. & Genant, H.K. (1998) High-resolution magnetic resonance imaging: three-dimensional trabecular bone architecture and biomechanical properties. *Bone*, **22**, 445–454.

Modlesky, C.M., Majumdar, S., Narasimhan, A. & Dudley, G.A. (2004) Trabecular bone microarchitecture is deteriorated in men with spinal cord injury. *J. Bone Miner. Res*. **19**, 48–55.

Mosekilde, Li. (1988) Age-related changes in vertebral trabecular bone architecture – assessed by a new method. *Bone*, **9**, 247–250.

Mosekilde, Li. (1989) Sex differences in age-related loss of vertebral trabecular bone mass and structure – biomechanical consequences. *Bone*, **10**, 425–432.

Mosekilde, Li. (1993) Vertebral structure and strength in vivo and in vitro. *Calcif. Tissue Int*. **53** (Suppl. 1), S121–S126.

Müller, R., Koller, B., Hildebrand, T., Laib, A., Gianolini, S. & Rüegsegger, P. (1996) Resolution dependency of microstructural properties of cancellous bone based on three-dimensional μ-tomography. *Technol. Health Care*, **4**, 113–119.

Müller, R., van Campenhout, H., van Damme, B., van der Perre, G., Dequeker, J., Hildebrand, T. & Rüegsegger, P. (1998) Morphometric analysis of human bone biopsies: a quantitative structural comparison of histological sections and micro-computed tomography. *Bone*, **23**, 59–66.

O'Keeffe, R.M. Jr, Riemer, B.L. & Butterfield, S.L. (1991) Harvesting of autogenous cancellous bone graft from the proximal tibial metaphysis. A review of 230 cases. *J. Orthop. Trauma*, **5**, 469–474.

Odgaard, A. (1997) Three-dimensional methods for quantification of cancellous bone architecture. *Bone*, **20**, 315–328.

Odgaard, A. & Gundersen, H.J.G. (1993) Quantification of connectivity in cancellous bone, with special emphasis on 3-D reconstructions. *Bone*, **14**, 173–182.

Parfitt, A.M. (1987) Trabecular bone architecture in the pathogenesis and prevention of fracture. *Am. J. Med*. **82**, 68–72.

Parfitt, A.M., Mathews, C.H.E., Villanueva, A.R., Kleerekoper, M., Frame, B. & Rao, D.S. (1983) Relationships between surface, volume, and thickness of iliac trabecular bone in aging and in osteoporosis. Implications for the microanatomic and cellular mechanisms of bone loss. *J. Clin. Invest*. **72**, 1396–1409.

Patel, V., Issever, A.S., Burghardt, A., Laib, A., Ries, M. & Majumdar, S. (2003) MicroCT evaluation of normal and osteoarthritic bone structure in human knee specimens. *J. Orthop. Res*. **21**, 6–13.

Rüegsegger, P., Koller, B. & Müller, R. (1996) A microtomographic system for the nondestructive evaluation of bone architecture. *Calcif. Tissue Int*. **58**, 24–29.

Sivarajasingam, V., Pell, G., Morse, M. & Shepherd, J.P. (2001) Secondary bone grafting of alveolar clefts: a densitometric comparison of iliac crest and tibial bone grafts. *Cleft. Palate Craniofac. J*. **38**, 11–14.

Stalling, D., Westerhoff, M. & Hege, H.-C. (2005) Amira: a highly interactive system for visual data analysis. *The Visualization Handbook* (ed. by C. D. Hansen and C. R. Johnson), pp. 749–767. Elsevier, Amsterdam.

Sterio, D.C. (1984) The unbiased estimation of number and sizes of arbitrary particles using the disector. *J. Microsc*. **134**, 127–136.

Thomsen, J.S., Ebbesen, E.N. & Mosekilde, Li. (2000) A new method of comprehensive static histomorphometry applied on human lumbar vertebral cancellous bone. *Bone*, **27**, 129–138.

Uchiyama, T., Tanizawa, T., Muramatsu, H., Endo, N., Takahashi, H.E. & Hara, T. (1997) A morphometric comparison of trabecular structure of human ilium between microcomputed tomography and conventional histomorphometry. *Calcif. Tissue Int*. **61**, 493–498.

Vico, L., Collet, P., Guignandon, A., Lafage-Proust, M.-H., Thomas, T., Rehailia, M. & Alexandre, C. (2000) Effects of long-term microgravity exposure on cancellous and cortical weight-bearing bones of cosmonauts. *Lancet*, **355**, 1607–1611.

Wehrli, F.W., Saha, P.K., Gomberg, B.R., Song, H.K., Snyder, P.J., Benito, M., Wright, A. & Weening, R. (2002) Role of magnetic resonance for assessing structure and function of trabecular bone. *Top. Magn. Reson. Imaging*, **13**, 335–355.

Weibel, E.R. (1980) *Stereological Methods*, Vol. 2. Academic Press, London.

Youngs, T.A., Boyce, R.W., Mosekilde, Li., Søgaard, C.H., Paddock, C.L. & Gundersen, H.J.G. (1994) Direct stereological estimation of 3-d connectivity density in human iliac cancellous bone: the effect of age and sex. *Acta Stereol*. **13**, 55–60.